AppliedChem

MDPI

Article

Biochar-Based Photothermal Membranes for Solar-Powered Distillation

Marcello Pagliero [1,2], Francesca Passaro [1], Antonio Comite [1,2], Ilaria Rizzardi [1], Lilia Longo [3], Giulia Forghieri [3,*] and Michela Signoretto [3]

[1] Department of Chemistry and Industrial Chemistry, University of Genoa, Via Dodecaneso 31, 16146 Genova, Italy; marcello.pagliero@unige.it (M.P.); francesca.passaro@edu.unige.it (F.P.); antonio.comite@unige.it (A.C.); ilaria.rizzardi@edu.unige.it (I.R.)
[2] INSTM, Udr di Genova, Via Dodecaneso 31, 16146 Genova, Italy
[3] CATMAT Lab, Department of Molecular Sciences and Nanosystems, Ca' Foscari University of Venice and INSTM RUVe, Via Torino 155, 30172 Venezia, Italy; lilia.longo@abo.fi (L.L.); miky@unive.it (M.S.)
* Correspondence: giulia.forghieri@unive.it; Tel.: +39-041-234-8552

Abstract

Biochar is a carbon-rich material produced from biomass pyrolysis whose properties can be tailored for various applications, including soil improvement, water purification, and catalysis. Its light absorption capacity also makes it promising for solar-driven processes like water evaporation. Photothermal membrane distillation (PMD) combines membrane separation with light-induced heating for efficient water purification. Unlike conventional membrane distillation, PMD utilizes light-absorbing materials to enhance vapor pressure and overcome temperature polarization, a common issue in membrane distillation. This study explored the potential of biochars and activated biochars, as filler materials for photothermal membranes, in line with circular economy principles. The mixed matrix membranes were prepared in a single step, via non-solvent induced phase separation starting from a uniform dispersion of the filler in a polyvinylidene fluoride solution. These materials exhibited great heating performance, reaching surface temperature up to 36 °C under a 125 W/m^2 light source. Increasing the biochar loading up to 15 wt.% resulted in an 85% increase in distillation flux under light irradiation.

Keywords: biochar; photo-thermal distillation; mixed matrix membranes

1. Introduction

Water is a critical resource whose availability and integrity are being increasingly threatened by various factors, including global warming [1]. In fact, besides the non-consumptive demand, human habitation needs to rely on an adequate supply of potable water [2]. Amongst the water treatment technologies, photothermal membrane distillation (PMD) could offer a sustainable approach to desalination, wastewater purification, and resource recovery [3,4]. PMD is a novel configuration of membrane distillation (MD) and is based on the creation of a vapor pressure gradient across a hydrophobic porous membrane, maintaining a temperature difference between the feed and permeate sides. As the feed solution is heated, water molecules evaporate and pass through the membrane pores, leaving behind concentrated solutes and non-volatile solutes [5]. The vapor then condenses on the permeate side, yielding a purified water stream.

PMD usually relies on the utilization of light-absorbing materials to convert light energy into localized heat, directly on the membrane surface. This additional heat source

Academic Editor: Svetlozar Velizarov

Received: 12 February 2026
Revised: 31 March 2026
Accepted: 22 April 2026
Published: 1 May 2026

can mitigate the temperature polarization (TP) phenomenon that significantly hinders the scaling up of MD systems [6]. TP consists of the decrease in the feed temperature in the boundary layer close to the membrane surface due to the evaporation of water and significantly reduces the effective driving force. Moreover, the feed bulk temperature tends to decrease along the module for the same reason, inducing practical limitations on the maximum length of the membrane module [7]. In general, PMD technologies face several limitations currently hindering their large-scale application. Issues like membrane wetting, fouling, salt accumulation, non-uniform light absorption and heat localization on the photothermal surface can significantly impair long-term stability and limit their practical integration into existing water treatment systems [4]. In addition, the incorporation of photothermal materials for membrane synthesis may also introduce additional challenges related to material durability, leaching, and scalability.

Photothermal membranes can be prepared by adding a dedicated layer on top of a traditional membrane [8,9], or by producing mixed matrix membranes (MMMs) [10,11]. The latter consists of a polymer matrix embedded with inorganic or organic fillers, offering a synergistic combination of the properties of both components [12,13]. MMMs combine the processability of polymers with the selectivity and functionality of inorganic fillers, offering enhanced permeability, selectivity, and improved resistance to wetting and fouling in membrane distillation. Moreover, MMMs provide the opportunity for a more versatile design, enabling the modulation of transport properties, surface chemistry, and morphology [14]. This flexibility enables their adaptation to a wide range of separation processes under challenging operating conditions. Commonly, polymers and fillers are selected to enhance the mechanical strength, selectivity, and permeability of MMMs compared to traditional polymeric membranes [15]. In addition, light-absorbing fillers like carbon nanotubes, graphene [11,16], metal nanoparticles [10,17], or semiconductors [18] can be integrated into a polymer matrix, thereby allowing heat generation directly on the membrane surface [19]. In any case, the selection of an adequate filler plays a key role in defining the membrane performance [20–22]. In general, the use of metallic particles can lead to various issues, such as particle leaching, low ambient stability, limited light spectrum absorption and elevated costs, further challenging the development of photothermal membranes of this type [23,24]. Similarly, organic photoactive materials can have drawbacks concerning both chemical stability and high pricing [25]. These limitations highlight the need to explore novel and more sustainable alternatives. In this context, carbon (C) is known as an excellent light-to-thermal conversion material due to its ability to absorb the entire light spectrum without any spectral reflection, and it has been previously observed to reach up to an 80% increase in photothermal efficiency [26]. C-based materials are usually cheap, available, biodegradable, and stable even at elevated temperatures [27,28]. Biochar (BC), a carbon-rich by-product of biomass pyrolysis, has also been explored as a cost-effective C-based solar absorber for water evaporation technologies due to its high light-absorptivity [29–32]. Composed mainly of carbon (65–90%) [33] and smaller amounts of heteroatoms (H, N, O, S) and ashes [34], BC can act as a carbon sink, also potentially contributing to reduced greenhouse gas emission [35]. Properties like surface area, functional group availability, and hydrophobicity, as well as the condensed aromatic ring structure, are all influenced by the biomass type and pyrolysis conditions employed [36,37]. In general, high BC yield is achieved during slow pyrolysis, which consists of high temperature treatments (>600 °C) under an inert atmosphere, low heating rates, (°C/min) and long residence times (minutes or hours) [38]. However, these treatments usually decrease the number of functional groups on the BC surface, increasing their hydrophobicity [39,40]. In order to improve the porosity and the surface area, activation treatments using physical (e.g., H_2O, CO_2) or chemical agents (e.g., KOH, H_3PO_4, $ZnCl_2$) can be performed after BC synthesis [41–43]. Feed-

stock composition also impacts BC properties: lignocellulosic materials like wood produce hydrophobic, high-surface-area BC [44], while non-lignocellulosic sources (e.g., sludge, manure, algae, etc.) [45] yield nitrogen-, sulphur-, and phosphorus-rich BCs [46].

Therefore, BC properties can be modulated by the appropriate selection of feedstock and process parameters and be adapted to a wide range of applications, such as electrodes [47], soil amendments [48–52] pollutant absorbers [53–56], and catalysts [57–63]. An ability to modulate structural and chemical processes, together with an increased awareness of BC potential are likely to determine the future success—and field—of its tailored application [48,64]. For example, BC's ability to absorb a wide portion of the light spectrum makes it a valuable candidate for its incorporation in films and membranes [65], including for solar water desalination purposes [31]. As BC can be derived from waste biomass, its utilization can help not only to develop low-cost and waste-efficient materials for water distillation purposes, but also to align with circular economy principles.

In this work, BCs derived from two different sources, namely a lignocellulosic biomass (hazelnut shells waste, HS) and a leathery biomass from the tannery industry (leather shaving waste, L) obtained by LIFE GOAST technology (Green Organic Agents for Sustainable Tanneries), along with the respective activated BCs—obtained by a physical activation treatment with steam at 850—were explored as more sustainable alternatives to the commonly used photothermal carbonaceous fillers, for the preparation of porous MMMs. Leather shaving waste is a solid by-product from a chromium-free tanning process, primarily composed of collagen fibers, proteins, and organic green polymers used as tanning agents. Despite not containing heavy metals, it is a hard-to -dispose type of waste that requires novel strategies to be transformed into a higher added value product. Hazelnut shell waste is a lignocellulosic biomass predominantly made up of lignin (40%), and holocellulose (cellulose and hemicellulose, 56%) [66]. It is a by-product abundantly available in Italy, the world's second-largest producer of hazelnuts (14.3%) [67]. Therefore, once characterized, the different prepared materials were tested for the desalination of water and their performance was compared to a commercial carbon. The developed membranes were designed, in accordance with circular economy principles, to achieve more affordable distillation technologies in line with the United Nations Sustainable Development Goals, such as Clean Water and Sanitation (SDG 6).

2. Materials and Methods

2.1. Biochar Preparation

Leather shaving wastes derive from a green, metal-free tannery process developed through the European project Life Goast (Green Organic Agents for Sustainable Tanneries, 16 ENV/IT000416) and they were supplied by Pasubio S.p.A, Arzignano, Vicenza, Italy. Hazelnut shells (Tonda Gentile Romana) were supplied by Fattoria Lucciano Soc. Agr. S.s, Civita Castellana, Viterbo, Italy.

Slow pyrolysis was performed as described in previous works [58,59]. Briefly, 40 g of biomass were placed into a laboratory-scale fixed bed quartz reactor in a vertical tubular oven (Carbolite EVT 12/450B, Verder Scientific, Bergamo, Italy), equipped with a mass flow controller (Brooks Instrument, Hatfield, PA, USA) for nitrogen and steam. The pyrolysis was carried out with a heating rate of 5 °C/min up to 700 °C for 30 min. The system was kept under inert atmosphere with a N_2 flow of 100 mL/min. The liquid fraction was condensed and collected out of the reactor, while the BC was formed into the quartz tube. The activation step was conducted at a temperature of 850 °C with a 10 °C/min heating ramp, for 90 min in a 1:1 N_2:steam atmosphere.

Leather tannery waste and hazelnut shell-derived BCs were labeled respectively B1 and B2, while the activated ones were labelled BA1 and BA2.

2.2. Biochar Characterizations

Scanning electron microscopy (SEM) was performed using a FE-SEM LEO 1525 ZEISS (Jena, Germany). The acceleration voltage was set to 15 keV, and imaging was conducted using a SE2 (Secondary Electron) detector and an In-lens detector. Samples were prepared by depositing them onto conductive carbon adhesive tape and sputter-coated with an 8 nm layer of chromium to enhance conductivity.

N_2 physisorption analysis was performed at −196 °C with Tristar II Plus Micromeritics. An amount of ca. 50 mg of BC was weighted and degassed at 0.15 mbar and 200 °C for 2 h (VacPrep 061 Micromeritics, Norcross, GA, USA). The surface area was calculated by the BET equation, and the pore volume was measured according to the adsorbed amount of N_2 at p/p0 near 0.98.

The contact angle of the samples was assessed with a digital tensiometer (Biolin Scientific Attention Theta, Helsinki, Finland). An amount of ca. 0.2 g of material was weighed and pressed with a hydraulic press into a 1 cm tablet. A 3 µL drop of water was deposited on the surface of the tablet using an automatic syringe. The water contact angle was recorded with an integrated camera for 10 s at 15 frames per second.

The CHNS elemental analysis of both BCs and activated BC was performed by a UNICUBE organic elemental analyzer (Elementar, Milano, Italy). Ashes amount was calculated by thermogravimetry (TGA 8000 Perkin Elmer, Waltham, MA, USA) following the ASTM-D7582 procedure. Oxygen percentage (Equation (1)) was calculated by difference as:

$$O\% = 100 - (C\% + H\% + N\% + S\% + Ash\%) \quad (1)$$

Fourier transformed Infrared Spectroscopy (FT-IR) analyses were conducted with a Perkin Elmer Spectrum one spectrophotometer in the 4000–400 cm^{-1} range, dispersing the powders in a KBr pellet. KBr (Spectroscopy grade, Merck, Darmstad, Germany) was used to disperse 0.05% of each BC, after drying in at 110 °C overnight. The mixture was pelletized to thin disks with a hydraulic press at 10 bar to allow the analysis. The spectra were collected with 40 scans at a resolution of 1 cm^{-1}.

2.3. Membrane Preparation

A certain amount of PVDF (Solef® 6010, Solvay Speciality Polymers, Alessandria, Italy, Mw 300 kDa) was dissolved in triethyl phosphate (TEP, Merck, Darmstad, Germany) to obtain the dope solutions for PVDF-based membranes. A different approach was used to obtain a better dispersion of the BC in the loaded membranes. First, a small amount of BC was finely ground in an agate grinder to minimize the particle size. Then, a precise amount of BC was placed in a 25 mL bottle and weighed on an analytical balance before adding 15 g of TEP. The bottle with the BC/TEP mix was then immersed in an ultrasonic bath for 30 min. After that, the dispersed mixture was added to a weighted amount of PVDF. With the addition of some TEP, the BC dispersion was transferred quantitatively to the PVDF powder. The quantity of TEP used was carefully chosen to reach the desired concentration of polymer in the solvent. Finally, the ternary system was put on a stirring plate at 70 °C for 8 h to help the dissolution of the PVDF.

The membranes were prepared following the protocol described in previous works [68,69]. A commercial non-woven support (PET Viledon® FO-2401, Freudenberg, Germany) was attached on a flat glass with adhesive tape and wetted with some drops of the solvent, to increase the adhesion with the polymer. A 350 µm dope film was cast using a doctor blade and the glass plate was immersed into an ethanol 96 *v*/*v*% coagulation bath at constant speed and left to precipitate for 2 h.

After separating the newly formed membrane from the glass plate, it was rinsed with water to remove the non-solvent and then dried at room temperature overnight. Table 1 reports the preparation conditions for the membranes.

Table 1. Membrane preparation conditions.

Sample	B1_75	BA1_75	B2_75	BA2_75	B2_150	BA2_150	Blank
Filler concentration *	7.5 wt%				15.0 wt%		0
PVDF concentration	14.5 wt%						
Solvent	Triethylphosphate (TEP)						
Non-solvent	Ethanol 96 v%						
Casting thickness	350 µm						

* With respect to PVDF amount.

2.4. Membrane Characterization

The photothermal properties of the synthesized membranes were measured by monitoring the temperature increase induced by irradiation with a 100 W solar spectrum LED light (Shenzhen Milyn Technology, Shenzhen, China). The samples were attached to an insulating surface with double-sided adhesive tape and placed under the light source at 9 cm. The surface temperature was recorded every 30 s for 10 min using an infrared thermometer (RS-8662, RS PRO, Selangor, Malaysia).

To evaluate the liquid entry pressure (LEP), the membranes were positioned in a suitable cell filled with water, where the liquid pressure was increased with compressed air and measured with a digital manometer (Digitron 2026P, Frosinone, Italy), until the first drop of water passed through the membrane. The correspondent pressure is the LEP.

The Liquid–Liquid Displacement Porosimetry (LLDP) was chosen as the method to evaluate the pore size and pore distribution of the membranes. For that, a porometer built in the laboratory and previously described elsewhere was used [70]. Water/1-Octanol were chosen as displacing and wetting liquid respectively (interfacial tension of 1-Octanol/water = 8.5 mN/m, at 20 °C [71]). After leaving the membranes in Octanol overnight, they were placed in a 76 mm^2 test cell, where pressure was applied by a water phase flux with a HPLC-pump (ISCO 260D) to displace the wetting liquid, i.e., the organic phase, from the membranes. For each membrane, the pore size was measured on three different samples.

The extent of the dispersion of BC in the polymeric matrix was evaluated through an optical microscope (AM4515T5 EDGE, Dino-lite, Almere, The Netherlands).

The membrane roughness was measured using a profilometer (MarSurf PS10, Mahr Gmbh, Goettingen, Germany). A small sample was stuck on a flat surface, and the roughness values were evaluated on three different zones for each sample.

2.5. Photothermal Membrane Distillation Tests

The PMD performance was assessed using a small setup, as schematized in Supplementary Materials Figure S1. The membrane cell was equipped with a transparent wall made of polymethylmethacrylate (PMMA) that allowed the passage of light to the photoactive membrane surface that is in contact with the feed.

The treated feed was a 30 g/L NaCl solution that was poured into a small tank at a temperature of 23 °C. The tank was equipped with a graduated pipette to avoid air bubbles and connected to a peristaltic pump. The feed flow rate was set at 40 mL/min (0.8 cm/s) and a light source (100 W solar spectrum LED light bulb, Shenzhen Milyn Technology, Shenzhen, China) was positioned 9 cm away from the active surface, resulting in an irradiance of 125 W/m^2 on the membrane surface. The distillate side of the cell (gray

in Figure S1) was maintained undersaturated with a constant flux of dry air at a rate of 10 L/min (220 cm/s). The graduated pipette was used to measure the feed volume decrease in a fixed time span to determine the distillate flux. The feed was continuously recirculated for 1 h, and two K-type thermocouples measured the water temperatures at the inlet and outlet of the cell. A digital data logger (HD2128.1, Deltaohm, Padova, Italy) was used to register the data just after the system reached a steady state, which took approximately 30 min.

A portion of the distilled water was condensed using an external cooler (not showed in Figure S1) and analyzed using an ion chromatograph (DX-120, Dionex, Sunnyvale, CA, USA) to determine the concentration of chloride ions and calculate the salt rejection.

3. Results

3.1. Biochar Properties

SEM analysis reported in Figure 1 revealed significant morphological differences among the samples. B1 exhibited a flat surface with no evident corrugations. Upon activation, BA1 developed small cavities, a few microns in size, while largely retaining its flat morphology. In contrast, B2 displayed a sponge-like structure characterized by ordered, elliptical cavities [72]. This porous structure derives from the decomposition of lignocellulosic biomass [59] which retains the structural integrity of plant cell walls, composed mainly of cellulose, lignin, and hemicellulose [73]. Activation further modified these cavities in BA2, enlarging them and altering their shape to more rounded forms, resulting in a highly corrugated surface [74].

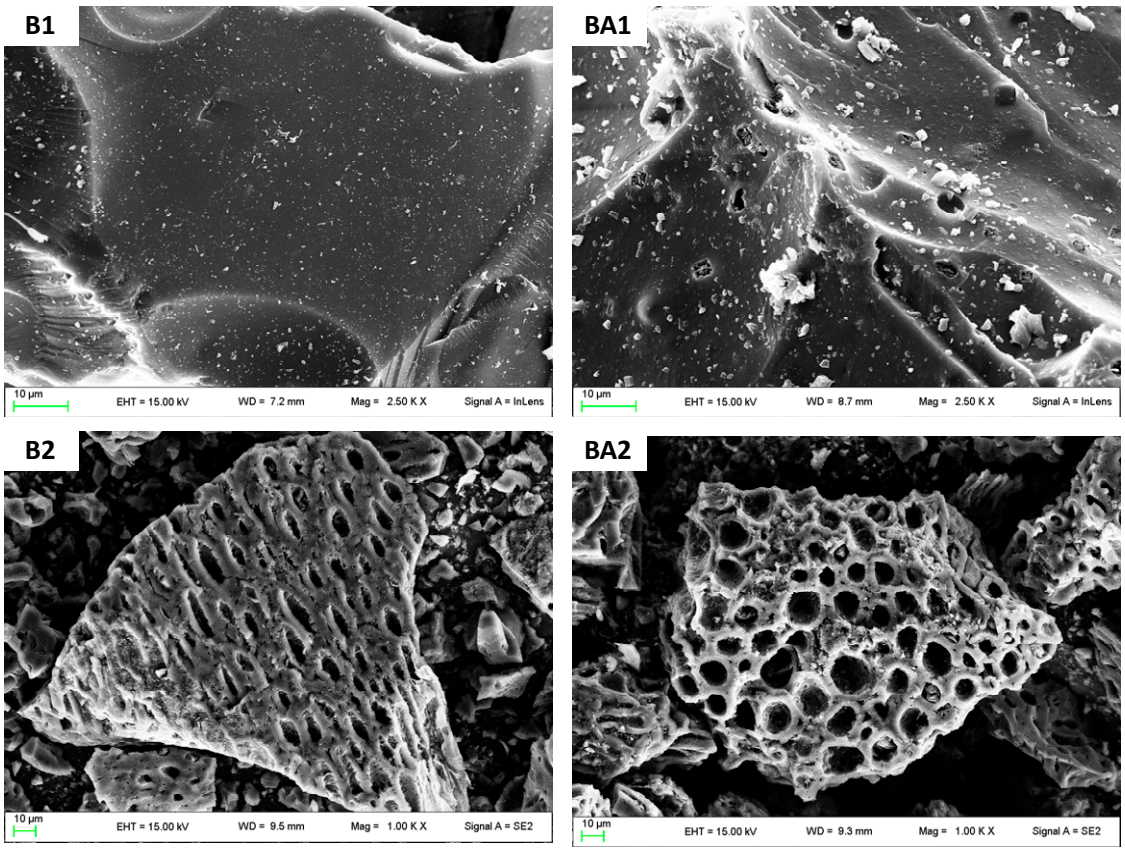

Figure 1. SEM images of the pristine biochar (**B1**,**B2**) and activated samples (**BA1**,**BA2**).

N_2 physisorption analyses also supported that the textural properties of the selected BCs were affected by the starting biomass and changed upon steam activation (Table 2).

While B1 sample showed poor porosity, acting as a non-porous material, the activation process was able to develop a microporosity in BA1, possibly by partial oxidation of the carbon structure by mean of reactions of carbon with H_2O to form CO and CO_2. A similar effect was observed for B2 and BA2, although this sample already displayed a moderate surface area. Therefore, the activation-dependent structural modifications observed by SEM analysis also reflected in the textural properties of both samples, displayed as increased surface area, reached up to 900 and 1100 g/m^2 for BA1 and BA2, respectively (Table 2). The morphological differences in the materials can be reconducted to the original biomass: the high percentage of lignin in hazelnut shells and the naturally organized hierarchical structure is retained in the char [75]. Indeed, BA2 showed the presence of both micro and mesopores. On the other hand, the carbonization process of a non-structured raw material like the shaving waste of leather, mainly composed of collagen and tanning agents, lead to a less porous material.

Table 2. Biochar characteristics.

Sample	B1	BA1	B2	BA2
Feedstock	Leather shaving waste		Hazelnut shells	
Treatment post pyrolysis	None	Steam activation at 850 °C	None	Steam activation at 850 °C
Surface area [m^2/g]	0 *	900	460	1100
Pore volume [cm^3/g]	0 *	0.25	0.20	0.31
C [%]	74.1	72.5	86.1	89
H [%]	1.6	1.9	2.2	0.9
N [%]	10.3	5.3	0.3	0.2
S [%]	1.1	0.7	0.1	0.1
O [%]	4.8	8.6	9.4	5.3
H/C	0.02	0.03	0.02	0.01
O/C	0.06	0.12	0.11	0.05
N/C	0.14	0.07	0.003	0.002
Ashes [%]	8.0	11.0	1.8	4.5

* Values below the instrumental lower detection limit.

Strong differences between the materials were also evidenced by the elemental analysis. Lignocellulosic BCs (B2 and BA2) presented a higher percentage of C, and a lower number of heteroatoms and ashes. The activation, in the case of BA2, caused an increase in C content resulting in the lowest H/C and O/C ratio, and indicating a more stable material with a highly ordered and more hydrophobic structure [76].

On the other hand, B1 and BA1 showed a higher quantity of heteroatoms, especially N, deriving from the proteins of the original biomass, as also supported by the higher N/C ratios compared to hazelnuts samples. In addition to oxygen, the presence of nitrogenated functionalities can contribute to the overall hydrophilicity and acidity of the system [77], potentially interacting with the polymer and hence influencing the matrix stabilization during the synthesis of the membrane. It is worth noting that the activation step had an opposite effect in terms of O% for the two biomasses. The high temperature treatment led to the dehydration and decomposition of the surface functionalities in BA2, while the development of a porous structure in BA1 was likely beneficial for the formation of new functionalities. For both feedstocks, the rising of temperature treatment led to an increased concentration of ashes due to the volatilization of the organic fraction.

The type and number of functionalities can play a role in the interaction with the polymer matrix when mixing the filler with the membrane [65]. Therefore, surface functionalities of the samples were investigated using FT-IR spectroscopy, as shown in Figure 2a,b. All samples exhibited similar characteristic peaks corresponding to various functional groups. Notably, in agreement with CHNS analysis, BA1 showed more pronounced signals

than B1 at 3414 cm^{-1}, 1580 cm^{-1}, and 1050 cm^{-1}, indicating the presence of oxygenated and nitrogenated functionalities (–OH, C=O, and C–O/C–N, respectively). In contrast, BA2 displayed weaker signals compared to B2, confirming a reduction in heteroatoms, as corroborated by elemental analysis.

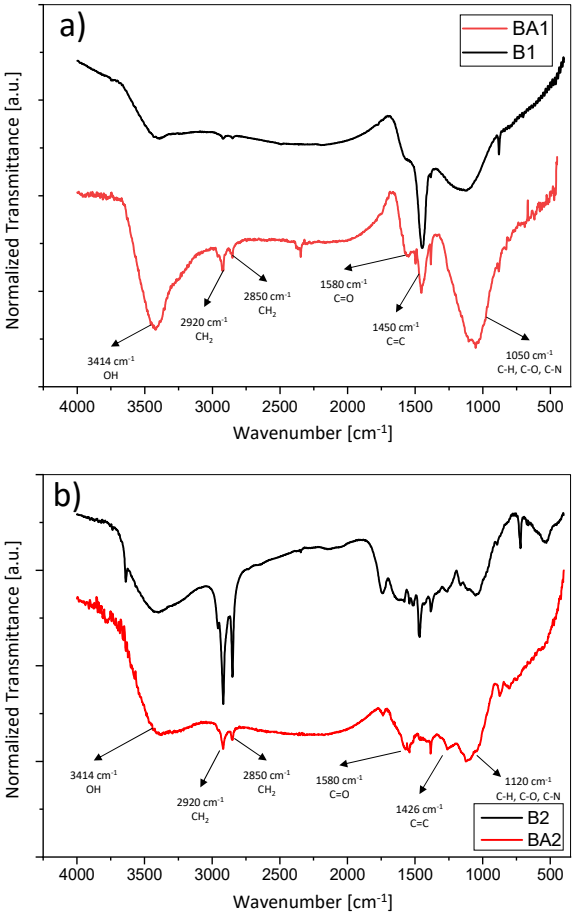

Figure 2. FT-IR spectra of (**a**) B1, BA1 and (**b**) B2, BA2.

The membranes for distillation applications must be porous and hydrophobic to let the water vapor pass while retaining the liquid phase and all the species dissolved in the feed. Consequently, the fillers should retain similar properties to achieve effective membrane synthesis. The addition of particles can alter the surface properties in two different ways: (I) by changing their morphology (e.g., modifying the roughness) or (II) by influencing their affinity with water. The water contact angle measurements performed on the B2 biochar sample are reported in Figure S2. In this case, the water drop rapidly and completely absorbed by the BC particles, indicating a strong affinity of the material with water, which could lead to a decrease in the hydrophobicity of the final MMM. The same phenomenon was observed for BA1 and BA2 samples. B1 acted slightly differently: after the deposition, the water droplet was absorbed gradually, over a longer time span. This difference was ascribed to the sensibly lower surface area and pore volume of the material, compared to the other fillers. The initial contact angle and the complete absorption times are summarized in Table S1.

3.2. Membrane Properties

Membranes were prepared by adding either 7.5% or 15% BC to the polymer solution. It was previously shown that increasing the carbon black concentration improved the light

absorbance of the membranes and boosted the feed temperature rise on the membrane surface [78].

For B1 and BA1 fillers, the highest possible amount added was 7.5 wt%, since larger loads created unstable dispersion in TEP during the preparation of the polymeric solution. For B2 and BA2 instead, it was possible to reach concentrations of up to 15 wt%. This outcome was likely attributed to the combination of the higher surface area and the more uniform particle dispersion of the HS-derived BC, both contributing to a more intimate interaction between the latter and the polymeric matrix (Figure S3).

Figure S3 shows the distribution of the particle size in the TEP dispersion, before the addition of PVDF while Figure 3 reports the size distribution of aggregates in the MMM. During the membrane formation, the dimension of the filler particles remained almost identical, ranging between 1 and 10 µm, thus confirming the stability of the particle dispersion in the dope solution. For each sample, 50 random particles were considered.

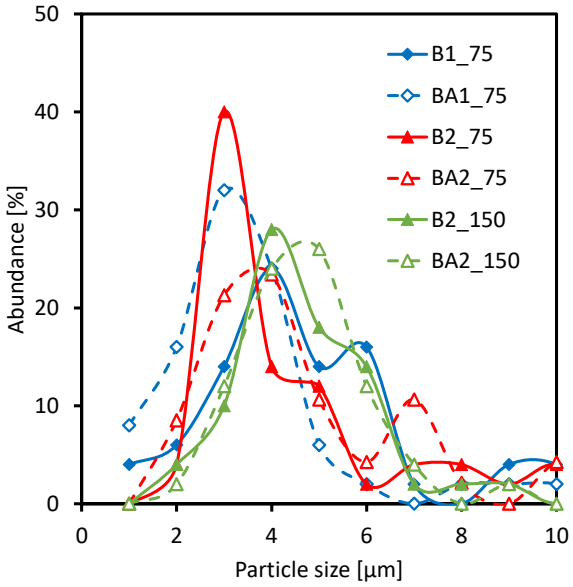

Figure 3. Aggregates size distribution.

The uniformity of the filler dispersion in the polymeric matrix and the existence of aggregates when using carbon-based particles was evaluated via optical microscopy. Figure 4 reports the images obtained at about 500X magnification for all the samples prepared together with a membrane without fillers (Figure 4G) and one prepared with a commercial carbon black (Figure 4H, Vulcan XC72R, Cabot Corp, Boston, MA, USA). The dispersion of the particles was more uniform for B2 and BA2 filled samples, although aggregates and some bigger particles were found in all samples (Figure 4).

The presence of larger aggregates could induce the formation of defects in the membrane structure. Increasing the loading of BC up to 15% led to greater aggregation phenomena, potentially affecting the homogeneity of particle distribution. In comparison, using a commercial filler characterized by smaller and more uniform particle size (30–60 nm carbon black, Figure 4H) it was possible to obtain a more uniform dispersion of the photoactive particles in the polymer matrix. Defects are one of the major problems in membrane development since they can allow the passage of liquid feed, reducing the separation ability of the process [79].

A simple measurement used to detect the defects is the evaluation of the LEP, which is defined as the lowest pressure required to force liquid water through the membranes. Low LEP values indicate a membrane with large defects while higher pressures mean that the membranes have small pores. Table 3 reports the values registered for the prepared membranes.

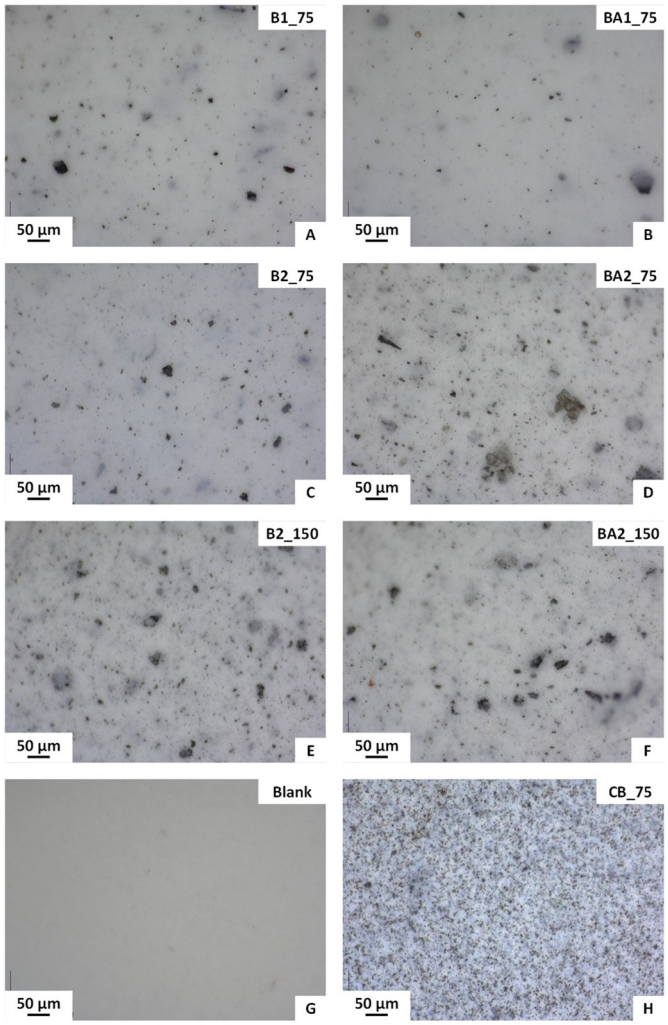

Figure 4. Optical micrographs of the membranes prepared (**A**–**F**), of a sample without filler. (**G**) and of a membrane containing 7.5 wt.% of carbon black (**H**).

Table 3. Water contact angle, average roughness, LEP, and mean pore size of the membranes.

Sample	Contact Angle [°]	Average Roughness [µm]	LEP [mbar]	Mean Pore Size [µm]
B1_75	145 ± 2	2.0 ± 0.3	850 ± 10	0.07
BA1_75	146 ± 5	1.4 ± 0.2	500 ± 20	0.10
B2_75	143 ± 1	1.7 ± 0.3	650 ± 30	0.04
BA2_75	141 ± 2	1.9 ± 0.7	350 ± 10	0.16
B2_150	140 ± 1	4.0 ± 0.7	940 ± 50	0.18
BA2_150	146 ± 5	4.7 ± 1.6	200 ± 30	0.21
Blank	147 ± 2	0.5 ± 0.1	1450 ± 80	0.22
CB_75	145 ± 6	-	4100 ± 300	0.86

In all cases, the addition of the filler reduced the LEP of the membrane and, particularly using BA1 and BA2 fillers, values as low as 200 mbar were registered. Such low LEP hinders the application of the membranes in vacuum membrane distillation (VMD) setups but may be acceptable for sweeping gas mode (SGMD). This configuration is characterized by an almost null transmembrane pressure and is then suitable for membranes with low LEP values.

Another parameter that must be evaluated prior to MD operation is membrane hydrophobicity. To prevent wetting phenomena and the flooding of the porous structure,

the membranes for MD must be hydrophobic. The evaluation of the water contact angle (CA) by means of the hydrophobicity index revealed that the differences observed for all the prepared membranes were quite marginal as all samples were characterized by high CA and were comparable to the values obtained with carbon black (Table 3). In this case, B2 and BA2 fillers seemed to slightly reduce the CA of the membranes. This effect was hypothetically attributed to the hydrophobicity of the HS-derived biochar, also expressed as low numbers of oxygen functionalities as suggested by FTIR analysis, while the high value registered for BA2_150 was likely influenced by the surface roughness induced on the surface by the increased aggregation phenomena.

3.3. Membrane Performance

One of the main features required for PMD application is the intensity of the photothermal effect induced by the inclusion of the filler in the polymer matrix. Figure 5 shows the surface temperature reached by the different samples when exposed to a simulated solar light.

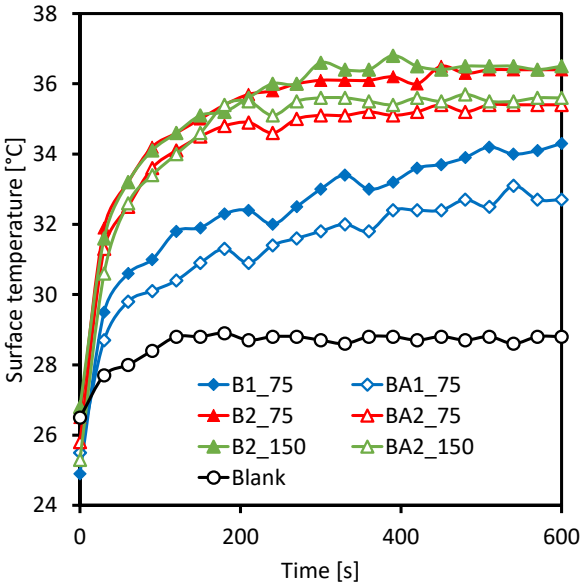

Figure 5. Membrane surface temperature under light irradiation.

Despite the poor dispersion of the filler and the light color of the membranes, the results were quite promising, especially using HS-based BC that reached a surface temperature almost 8 °C higher than the blank sample. Considering that the light source had an irradiance of approximately 125 W/m^2 (compared to 1000 W/m^2 of the sun at midday), 36 °C is an excellent value, absolutely in line with what was previously recorded using carbon black [78]. Furthermore, it was observed that exceeding a certain concentration of fillers in the membrane does not result in large increases in ability to absorb energy and transform it into heat. The temperature increase obtained with both B2 and BA2 is consistent with what was previously observed for a biochar-based membrane derived from rice husks, tested for distillation purposes [32]. The activation treatment apparently had a slightly negative—although still modest—effect on the overall performance.

The membranes with adequate properties were then tested in the SGMD setup, both with no light irradiation and under a simulated solar light. BA2_150 membrane was affected by pore flooding and feed leaking phenomena due to the low LEP related to the presence of defects, as discussed above. The results collected for all the other membranes are reported in Figure 6.

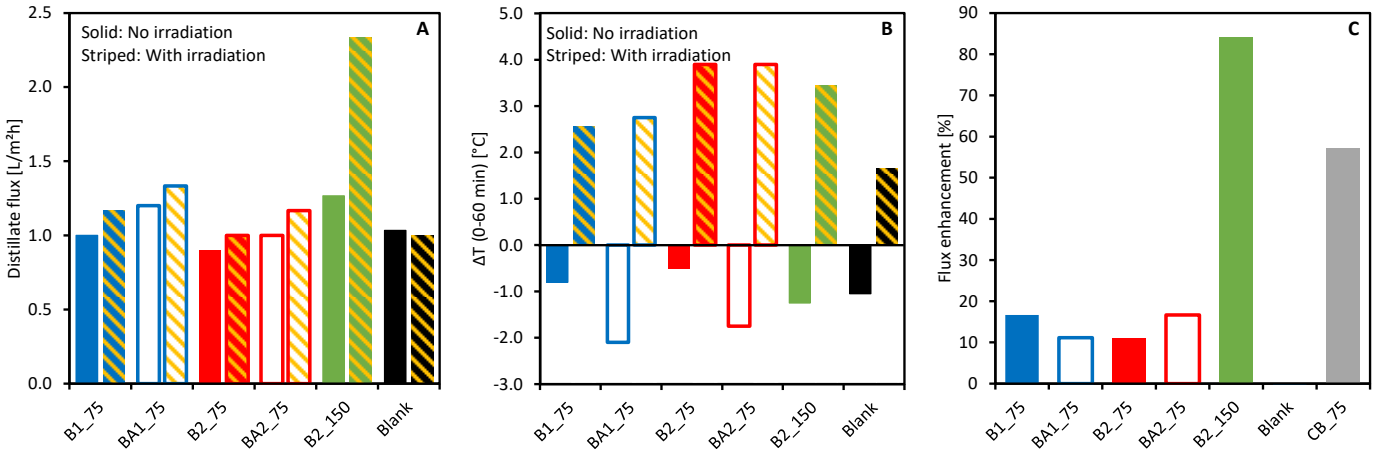

Figure 6. (**A**) SGMD distillation flux without (solid) and with (striped) light irradiation; (**B**) Feed temperature difference between the start and the end of the PMD test and (**C**) relative percent flux enhancement under irradiation.

4. Discussion

The SGMD tests performed without light irradiation (solid bars in Figure 6) showed the variable influence of the addition of the filler on the permeate flux. For each test, small aliquots of the permeate were condensed and analyzed with an ion-chromatograph to evaluate the amount of chloride ions. All the samples were characterized by a Cl concentration lower than 1 ppm, confirming the complete rejection of salt during the distillation process. The membranes were able to withstand the operation conditions, and the porous structure was not flooded by the liquid feed. However, in long term operations, the membranes prepared in this work could suffer wetting problems induced by the high hydrophilicity of the filler and the suboptimal dispersion in the polymer matrix. Further research to reduce the particle size and optimize the biochar functional groups will be required.

At low concentrations the unmodified BC induced a slight decrease in the distillation flux in comparison with the blank membrane that is probably related to the reduction in pore size. The distillation fluxes obtained were comparable to the one detected for biochar-based membranes in similar distillation technologies, also situated in the range of 1.3–1.5 L/m^2 h [31]. However, when the BC content was doubled, the distillate flux increased by 60% for B2.

The ability to convert sunlight into heat during the PMD tests can also be confirmed by the bulk temperature changes between the start and the end of the tests, reported in Figure 6B. During the tests performed without light irradiance, the feed temperature decreased between the start and the end of the distillation because of the latent heat removal correlated with water evaporation. However, this trend was inverted when the membranes were irradiated.

For all the samples, the PMD tests confirmed the activity of the composite membranes (Figure 6C). In fact, while the blank membrane was completely uninfluenced by the light irradiation, the samples that contained the carbon-based filler showed an increase in the distillation flux.

Nevertheless, due to the different experimental conditions, a direct comparison of the distillation performance of the membranes prepared in this work with the one presented in previous studies is not possible. In fact, the CB loaded membrane investigated previously [80] had a higher LEP (see Table 3) and was tested using a PMD setup operating in vacuum mode. However, it is possible to compare the flux enhancement factor, as reported

in Figure 6C. In this case, B2_150 showed the highest increase with a distillation flux under irradiation that was almost 90% higher than the one with no light (Figure 6C).

The CB loaded membrane showed a distillation flux increase of around 60% with a filler concentration of 7.5 wt%. The BC-based samples obtained with the same filler concentration reached a flux enhancement of only 15%, possibly because of the less homogenous filler dispersion, as observed above.

If compared with similar C-based MMMs, the sample B2_150 prepared in this study showed either comparable or superior performances (Table 4). A flux of 2.4 L/m^2 h was considered promising if considering the low irradiance utilized with respect to other studies. In addition, although the preparation of biochar-based MMMs has been previously proposed for water remediation purposes [16,81], the effective application of this type of MMMs for PMD technologies has not been previously reported to the best of our knowledge, preventing a more accurate comparison in this context.

Table 4. Distillate flux of different MMMs with C-based fillers for PMD applications. Where CNT stands for carbon nanotubes, CB for carbon black, BC for biochar, GT for graphite and GN for graphene.

Sample	Flux ($L/m^2 \cdot h$)	Irradiance (W/m^2)	System	Reference
15% BC/PVDF (B2_150)	2.4	125	PMD	This work
25% CB/PVDF	0.3	160	PMD	[78]
1% CNT/PSF	5.6	1100	PMD	[82]
7.5% GT/PVDF	1.8			
7.5% GN/PVDF	1.9	675	PMD	[83]
7.5% CB/PVDF	2.3			
20% CNT/PVDF	0.4	1000	PMD	[84]

In this case, with a lower filler amount (7.5 wt.%), B1 and B2 showed very different behaviors both relative to the T and flux enhancements, which were ascribed to the different BC properties. Figure 7a displays the different measured properties of activated and non-activated BCs, while Figure 7b shows the resulting BC-based membrane properties. The thermal activation process increased the surface area and pores volume along with the O/C ratio of B1. These features were related to a decreased hydrophobicity, negatively impacting the interaction with the polymer matrix. These features are likely reflected in both the lower distillation flux (Figure 6) and the decreased membrane performance observed for BA1_75 compreflected5. In the case of B2, the activation process decreased the O/C ratio, thereby also resulting in a higher flux enhancement of BA2_75 compared to B2_75. Besides affecting the membrane performance, the characteristics of BCs were found to be relevant to determine the loading percentage of the filler. In this regard, it was observed that a more hydrophobic BC, such as HS-biochar, was more easily introduced in the polymeric matrix thereby enabling the integration of larger amounts of filler in the membrane. Hence, increasing the amount of filler (i.e., 15 wt%) produced a better flux increase, as reported in Figure 6. In this case, the higher surface area measured for B2 is also believed to have positively influenced the integration of the filler within the membrane, accounting for the higher spatial interaction of the BC with the polymer matrix. In this regard, the observed results helped to explain the limitations on the loading rate of B1 and BA1 into the final MMM. The difficulty in integrating B1/BA1 into the polymer matrix was attributed to two main factors: (1) the higher hydrophilicity of the system due to the presence of N functionalities and (2) the morphological properties related both to porosity, roughness, and the particle size of the material, as also evidenced by SEM analyses (Figure 1). In fact, larger or more irregular biochar particles can lead to the formation of aggregates reducing the quality of dispersion [84]. Hence, both factors would result in a reduced interaction

with the polymer, also explaining the lower rates of filler loading obtainable for B1 and BA1 (7.5%) compared to B2 and BA2 (15%).

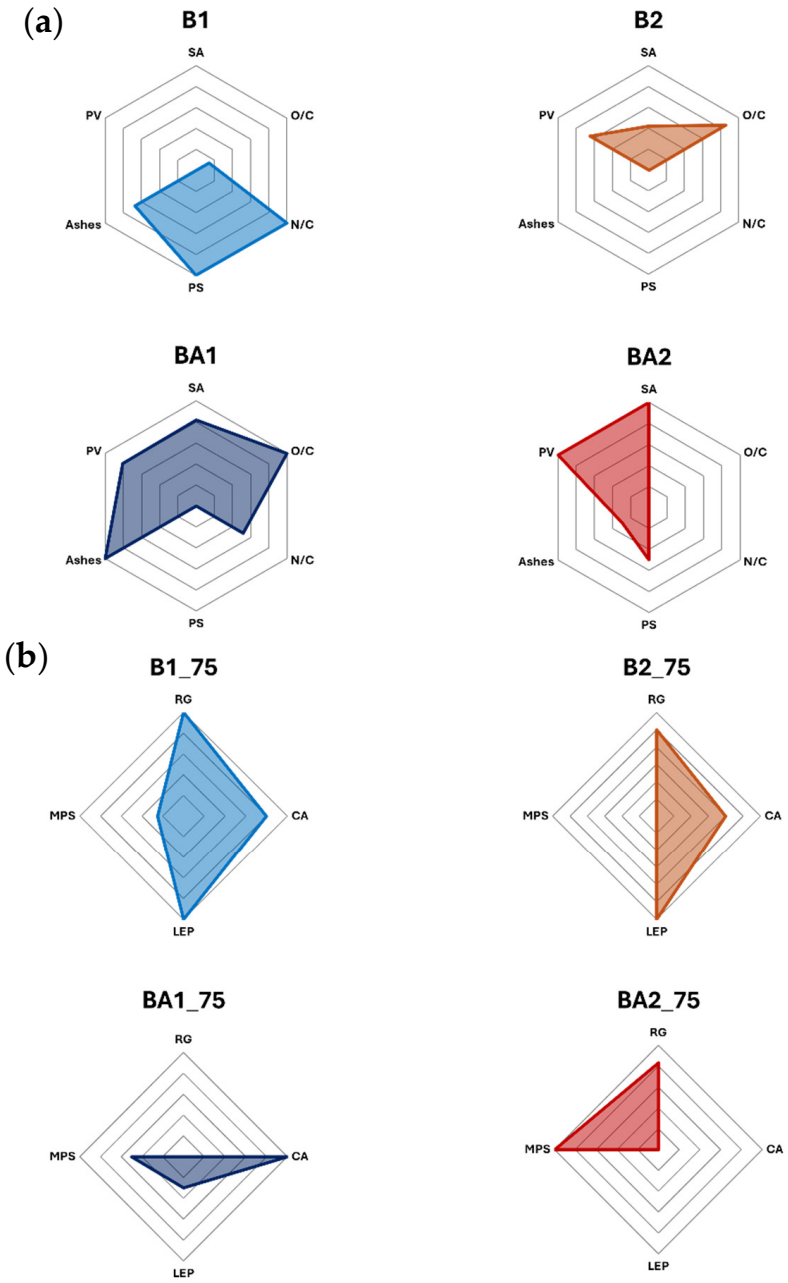

Figure 7. (**a**) Normalized properties of different BCs. PV: Pore volume; SA: Surface area; O/C: oxygen to carbon ratio; N/C: nitrogen to carbon ratio; PS: average particle size. (**b**) Normalized properties of different BC-based membranes. RG: Roughness; MPS: Medium pores size; LEP: liquid entry pressure; CA: Contact angle.

The interaction between the polymer chains and the filler particles can affect the solidification of the membrane. Therefore, the possibility to tune structural and textural features like porosity and hydrophobicity make waste-derived BC a promising candidate for effective MMMs design. Previous reports have demonstrated that nanofillers in the PVDF matrix worked as nucleation agents during phase formation [85]. In every condition, the addition of the filler reduced the size of the pore. This result was linked to the increase in the viscosity of the polymer solution which limits the mobility of the chains and favors the formation of surface layers. At low concentrations the added filler influenced the

thermodynamic stability of the dope solution and induced a faster precipitation rate during phase separation. At high concentrations the filler causes a most noticeable rise in the solution viscosity and a delay in the phase separation, with a restricted pore growth [86]. The presence of filler aggregates in MMM is known to influence mechanical integrity. If the polymer–filler interface adhesion is limited it can lead to mechanical weak spots eventually resulting in crack initiation and propagation under shear or pressure-driven flow conditions [87]. However, at moderate loadings and with good interfacial compatibility, fillers can reinforce the membrane matrix and improve mechanical stability. In the synthesized systems, leather-derived biochar tended to aggregate at higher loadings potentially leading to reduced mechanical homogeneity compared to hazelnut shell-derived biochar, which showed better dispersion. The obtained results suggested that modulating the BC properties, such as the O/C ratio, via either process parameter modification or biomass selection, along with the modulation of particle size can be used as strategy to design more effective and reliable MMMs to be used in scalable photo-driven distillation technologies.

5. Conclusions

In this work, waste-derived BCs and activated BCs obtained from lignocellulosic residue, hazelnut shells, and an industrial by-product, leather shaving waste, were used as more sustainable fillers for the preparation of photothermal membranes following the principles of circular economy, aiming at contributing to the UN SDGs.

The samples prepared were comparable with the heating performance of mixed matrix membranes prepared with commercial carbon black, with the biochar with the highest lignocellulosic content showing the best performance.

In comparison with conventional carbon black loaded membranes, using biochar it was possible to increase the concentration of the filler within the polymeric matrix leading to an improved flux enhancement factor under simulated sunlight.

In particular, it was shown that BCs properties differently affected the membrane performance. As MMMs synthesis relies on the interaction between the polymer matrix and the filler, the possibility to modulate its structural and textural features make waste-derived BC a valuable candidate for designing more effective PMD. Advancements in ability to control particle size and dispersion are expected to further improve BC performance as filler, and therefore its utilization in this field. Hence, future work should focus on optimizing the dimension of the filler particles, to avoid undesired effects on the membrane properties, such as a poor dispersion in the polymeric matrix and a decrease in LEP values potentially preventing the use of vacuum membrane distillation mode. Rheological studies can be performed to further confirm the interaction between the filler and the polymer and to help guide the matrix design. Finally, the results obtained suggest that integrating BCs in PMD technologies may represent a viable opportunity for the valorization of this type of waste for highly valued purposes, although further studies to reduce the particle size and surface hydrophilicity are required. Being produced in line with circular economy principles, developing biochar-based membranes complies with the opportunity to design more affordable distillation technologies with overall reduced waste and environmental impact. Future studies should aim to optimize BC properties in order to improve stress resistance and assess the industrial-scale application of these types of MMMs.

Supplementary Materials: The following supporting information can be downloaded at: https://www.mdpi.com/article/10.3390/appliedchem6020029/s1, Figure S1: PMD setup used for the distillation test; Figure S2: Contact angle measured on BA1 sample; Figure S3: Particle size in TEP dispersion; Table S1: Initial contact angle and water drop absorption time for biochar samples.

Author Contributions: Conceptualization: G.F. and M.P.; methodology: M.P.; investigation: F.P., I.R. and L.L.; writing—original draft preparation: M.P. and G.F.; writing—review and editing: M.S., F.P. and L.L.; supervision: A.C. and M.S. All authors have read and agreed to the published version of the manuscript.

Funding: This research received no external funding.

Institutional Review Board Statement: Not applicable.

Informed Consent Statement: Not applicable.

Data Availability Statement: All data supporting the findings of this study are available within the paper.

Acknowledgments: The authors would like to acknowledge Pasubio S.p.A, Arzignano, Vicenza, Italy and Fattoria Lucciano Soc. Agr. S.s, Civita Castellana, Viterbo, Italy for providing the raw materials for biochar preparation. Alessandro di Michele is kindly acknowledged for performing the SEM analyses used in this work.

Conflicts of Interest: The authors declare no conflicts of interest.

Abbreviations

The following abbreviations are used in this manuscript:

PMD	Photothermal membrane distillation
MD	membrane distillation
MMM	Mixed matrix membranes
BC	Biochar
VMD	Vacuum membrane distillation
SGMD	sweeping gas mode distillation
HS	Hazelnuts
LEP	Liquid entry pressure
LLDP	Liquid–liquid displacement porosimetry
TEP	Triethylphosphate
TP	Temperature polarization

References

1. Jeppesen, E.; Brucet, S.; Naselli-Flores, L.; Papastergiadou, E.; Stefanidis, K.; Nõges, T.; Nõges, P.; Attayde, J.L.; Zohary, T.; Coppens, J.; et al. Ecological Impacts of Global Warming and Water Abstraction on Lakes and Reservoirs Due to Changes in Water Level and Related Changes in Salinity. *Hydrobiologia* **2015**, *750*, 201–227. [CrossRef]
2. Lettenmaier, D.P.; Wood, A.W.; Palmer, R.N.; Wood, E.F.; Stakhiv, E.Z. Water Resources Implications of Global Warming: A U.S. Regional Perspective. *Clim. Change* **1999**, *43*, 537–579. [CrossRef]
3. Razaqpur, A.G.; Wang, Y.; Liao, X.; Liao, Y.; Wang, R. Progress of Photothermal Membrane Distillation for Decentralized Desalination: A Review. *Water Res.* **2021**, *201*, 117299. [CrossRef]
4. Gao, M.; Peh, C.K.; Meng, F.L.; Ho, G.W. Photothermal Membrane Distillation toward Solar Water Production. *Small Methods* **2021**, *5*, 2001200. [CrossRef]
5. Alkhudhiri, A.; Darwish, N.; Hilal, N. Membrane Distillation: A Comprehensive Review. *Desalination* **2012**, *287*, 2–18. [CrossRef]
6. Martínez-Díez, L.; Vázquez-González, M.I. Temperature and Concentration Polarization in Membrane Distillation of Aqueous Salt Solutions. *J. Membr. Sci.* **1999**, *156*, 265–273. [CrossRef]
7. Anvari, A.; Azimi Yancheshme, A.; Kekre, K.M.; Ronen, A. State-of-the-Art Methods for Overcoming Temperature Polarization in Membrane Distillation Process: A Review. *J. Membr. Sci.* **2020**, *616*, 118413. [CrossRef]
8. Huang, J.; Hu, Y.; Bai, Y.; He, Y.; Zhu, J. Novel Solar Membrane Distillation Enabled by a PDMS/CNT/PVDF Membrane with Localized Heating. *Desalination* **2020**, *489*, 114529. [CrossRef]
9. Wu, X.; Jiang, Q.; Ghim, D.; Singamaneni, S.; Jun, Y.S. Localized Heating with a Photothermal Polydopamine Coating Facilitates a Novel Membrane Distillation Process. *J. Mater. Chem. A* **2018**, *6*, 18799–18807. [CrossRef]
10. Politano, A.; Argurio, P.; Di Profio, G.; Sanna, V.; Cupolillo, A.; Chakraborty, S.; Arafat, H.A.; Curcio, E. Photothermal Membrane Distillation for Seawater Desalination. *Adv. Mater.* **2017**, *29*, 1603504. [CrossRef]

11. Wu, J.; Zodrow, K.R.; Szemraj, P.B.; Li, Q. Photothermal Nanocomposite Membranes for Direct Solar Membrane Distillation. *J. Mater. Chem. A* **2017**, *5*, 23712–23719. [CrossRef]
12. Dechnik, J.; Gascon, J.; Doonan, C.J.; Janiak, C.; Sumby, C.J. Mixed-Matrix Membranes. *Angew. Chem. Int. Ed.* **2017**, *56*, 9292–9310. [CrossRef] [PubMed]
13. Pagliero, M.; Khayet, M.; García-Payo, C.; García-Fernández, L. Hollow Fibre Polymeric Membranes for Desalination by Membrane Distillation Technology: A Review of Different Morphological Structures and Key Strategic Improvements. *Desalination* **2021**, *516*, 115235. [CrossRef]
14. Xue, Q.; Lim, Y.J.; Zhang, K. Recent Advances in MXene-Polymer Hybrid Membranes for Water Purification: From Interface Design to Functional Regulation and Transport Mechanisms. *Coord. Chem. Rev.* **2026**, *557*, 217723. [CrossRef]
15. Shi, W.; Xu, C.; Cai, J.; Wu, S. Advancements in Material Selection and Application Research for Mixed Matrix Membranes in Water Treatment. *J. Environ. Chem. Eng.* **2023**, *11*, 111292. [CrossRef]
16. Hameed, A.M.; Alayyafi, A.A.; Alluhaybi, A.A.; Fahmi, M.S.; Ali, M.E.A. Photothermal Efficiency of Carbon Nanotubes-Embedded Polysulfone Membranes for Direct Contact Membrane Distillation. *Iran. Polym. J.* **2024**, *33*, 1369–1380. [CrossRef]
17. Ye, H.; Li, X.; Deng, L.; Li, P.; Zhang, T.; Wang, X.; Hsiao, B.S. Silver Nanoparticle-Enabled Photothermal Nanofibrous Membrane for Light-Driven Membrane Distillation. *Ind. Eng. Chem. Res.* **2019**, *58*, 3269–3281. [CrossRef]
18. Ghim, D.; Jiang, Q.; Cao, S.S.; Singamaneni, S.; Jun, Y.S. Mechanically Interlocked 1T/2H Phases of MoS2 Nanosheets for Solar Thermal Water Purification. *Nano Energy* **2018**, *53*, 949–957. [CrossRef]
19. Subrahmanya, T.M.; Austria, H.F.M.; Chen, Y.Y.; Setiawan, O.; Widakdo, J.; Kurkuri, M.D.; Hung, W.S.; Hu, C.C.; Lee, K.R.; Lai, J.Y. Self-Surface Heating Membrane Distillation for Sustainable Production of Freshwater: A State of the Art Overview. *Prog. Mater. Sci.* **2024**, *145*, 101309. [CrossRef]
20. Dong, X.; Xu, L.; Ma, J.; Li, Y.; Yin, Z.; Chen, D.; Wang, Q.; Han, J.; Qiu, J.; Yang, Z.; et al. Enhanced Interfacial Charge Transfer and Photothermal Effect via In-Situ Construction of Atom Co-Sharing Bi Plasmonic/Bi4O5Br2 Nanosheet Heterojunction towards Improved Full-Spectrum Photocatalysis. *Chem. Eng. J.* **2023**, *459*, 141557. [CrossRef]
21. He, F.; Chen, H.; Li, J.; Zhao, C.; Zhang, J.; Wang, S. Photothermal-Mediated Advanced Oxidation Processes for Wastewater Purification. *Curr. Opin. Chem. Eng.* **2024**, *45*, 101039. [CrossRef]
22. Pan, Z.; Mao, Y.; Ai, X.; Cheng, H.; Li, W.; Cheng, F. Photothermal Membranes for Water Treatment and Anti-Fouling Performances: A Review. *J. Clean. Prod.* **2023**, *412*, 137335. [CrossRef]
23. Fuzil, N.S.; Othman, N.H.; Alias, N.H.; Marpani, F.; Othman, M.H.D.; Ismail, A.F.; Lau, W.J.; Li, K.; Kusworo, T.D.; Ichinose, I.; et al. A Review on Photothermal Material and Its Usage in the Development of Photothermal Membrane for Sustainable Clean Water Production. *Desalination* **2021**, *517*, 115259. [CrossRef]
24. Zhu, L.; Tian, L.; Jiang, S.; Han, L.; Liang, Y.; Li, Q.; Chen, S. Advances in Photothermal Regulation Strategies: From Efficient Solar Heating to Daytime Passive Cooling. *Chem. Soc. Rev.* **2023**, *52*, 7389–7460. [CrossRef]
25. Lv, S.; Miao, Y.; Liu, D.; Song, F. Recent Development of Photothermal Agents (PTAs) Based on Small Organic Molecular Dyes. *ChemBioChem* **2020**, *21*, 2098–2110. [CrossRef] [PubMed]
26. Shaheen, A.; AlBadi, S.; Zhuman, B.; Taher, H.; Banat, F.; AlMarzooqi, F. Photothermal Air Gap Membrane Distillation for the Removal of Heavy Metal Ions from Wastewater. *Chem. Eng. J.* **2022**, *431*, 133909. [CrossRef]
27. Alqaydi, M.; Mavukkandy, M.O.; Mustafa, I.; Alnuaimi, A.; Arafat, H.A.; Almarzooqi, F. Activated Carbon as a Photothermal Absorber in PVDF Membranes for Solar Driven Air-Gap Membrane Distillation. *Desalination* **2022**, *541*, 116031. [CrossRef]
28. Liao, X.; Dai, P.; Wang, Y.; Zhang, X.; Liao, Y.; You, X.; Razaqpur, A.G. Engineering Anti-Scaling Superhydrophobic Membranes for Photothermal Membrane Distillation. *J. Membr. Sci.* **2022**, *650*, 120423. [CrossRef]
29. Hota, S.K.; Diaz, G. Assessment of Pyrolytic Biochar as a Solar Absorber Material for Cost-Effective Water Evaporation Enhancement. *Environ. Eng. Sci.* **2021**, *38*, 1120–1128. [CrossRef]
30. Yang, L.; Chen, G.; Zhang, N.; Xu, Y.; Xu, X. Sustainable Biochar-Based Solar Absorbers for High-Performance Solar-Driven Steam Generation and Water Purification. *ACS Sustain. Chem. Eng.* **2019**, *7*, 19311–19320. [CrossRef]
31. Ghaffar, A.; Usman, M.; Khan, M.U.; Hassan, M. Simultaneous Solar Steam and Electricity Generation from Biochar Based Photothermal Membranes. *J. Clean. Prod.* **2024**, *446*, 141374. [CrossRef]
32. Liew, C.M.; Puteh, M.H.; Othman, M.H.D.; Kamaludin, R.; Jasman, S.M.; Asogan, P.; Muhammad, M.S. Rice Husk-Derived Photothermal Materials for Membrane Distillation. *Mater. Chem. Phys.* **2024**, *327*, 129837. [CrossRef]
33. Cheng, F.; Li, X. Preparation and Application of Biochar-Based Catalysts for Biofuel Production. *Catalysts* **2018**, *8*, 346. [CrossRef]
34. Pereira Lopes, R.; Astruc, D. Biochar as a Support for Nanocatalysts and Other Reagents: Recent Advances and Applications. *Coord. Chem. Rev.* **2021**, *426*, 213585. [CrossRef]
35. Matuštík, J.; Pohořelý, M.; Kočí, V. Is Application of Biochar to Soil Really Carbon Negative? The Effect of Methodological Decisions in Life Cycle Assessment. *Sci. Total Environ.* **2022**, *807*, 151058. [CrossRef] [PubMed]
36. Boguta, P.; Sokołowska, Z.; Skic, K.; Tomczyk, A. Chemically Engineered Biochar—Effect of Concentration and Type of Modifier on Sorption and Structural Properties of Biochar from Wood Waste. *Fuel* **2019**, *256*, 115893. [CrossRef]

37. Luo, L.; Xu, C.; Chen, Z.; Zhang, S. Properties of Biomass-Derived Biochars: Combined Effects of Operating Conditions and Biomass Types. *Bioresour. Technol.* **2015**, *192*, 83–89. [CrossRef]
38. Pituello, C.; Francioso, O.; Simonetti, G.; Pisi, A.; Torreggiani, A.; Berti, A.; Morari, F. Characterization of Chemical–Physical, Structural and Morphological Properties of Biochars from Biowastes Produced at Different Temperatures. *J. Soils Sediments* **2015**, *15*, 792–804. [CrossRef]
39. Uroić Štefanko, A.; Leszczynska, D. Impact of Biomass Source and Pyrolysis Parameters on Physicochemical Properties of Biochar Manufactured for Innovative Applications. *Front. Energy Res.* **2020**, *8*, 138. [CrossRef]
40. de Mendonça, F.G.; da Cunha, I.T.; Soares, R.R.; Tristão, J.C.; Lago, R.M. Tuning the Surface Properties of Biochar by Thermal Treatment. *Bioresour. Technol.* **2017**, *246*, 28–33. [CrossRef]
41. Panwar, N.L.; Pawar, A. Influence of Activation Conditions on the Physicochemical Properties of Activated Biochar: A Review. *Biomass Convers. Biorefin.* **2022**, *12*, 925–947. [CrossRef]
42. Anto, S.; Sudhakar, M.P.; Shan Ahamed, T.; Samuel, M.S.; Mathimani, T.; Brindhadevi, K.; Pugazhendhi, A. Activation Strategies for Biochar to Use as an Efficient Catalyst in Various Applications. *Fuel* **2021**, *285*, 119205. [CrossRef]
43. Lu, Z.; Zhang, H.; Shahab, A.; Zhang, K.; Zeng, H.; Bacha, A.U.R.; Nabi, I.; Ullah, H. Comparative Study on Characterization and Adsorption Properties of Phosphoric Acid Activated Biochar and Nitrogen-Containing Modified Biochar Employing Eucalyptus as a Precursor. *J. Clean. Prod.* **2021**, *303*, 127046. [CrossRef]
44. Kane, S.; Ulrich, R.; Harrington, A.; Stadie, N.P.; Ryan, C. Physical and Chemical Mechanisms That Influence the Electrical Conductivity of Lignin-Derived Biochar. *Carbon Trends* **2021**, *5*, 100088. [CrossRef]
45. Li, D.C.; Jiang, H. The Thermochemical Conversion of Non-Lignocellulosic Biomass to Form Biochar: A Review on Characterizations and Mechanism Elucidation. *Bioresour. Technol.* **2017**, *246*, 57–68. [CrossRef]
46. Fahmy, T.Y.A.; Fahmy, Y.; Mobarak, F.; El-Sakhawy, M.; Abou-Zeid, R.E. Biomass Pyrolysis: Past, Present, and Future. *Environ. Dev. Sustain.* **2020**, *22*, 17–32. [CrossRef]
47. Salimi, P.; Tieuli, S.; Taghavi, S.; Venezia, E.; Fugattini, S.; Lauciello, S.; Prato, M.; Marras, S.; Li, T.; Signoretto, M.; et al. Sustainable Lithium-Ion Batteries Based on Metal-Free Tannery Waste Biochar. *Green Chem.* **2022**, *24*, 4119–4129. [CrossRef]
48. Kamali, M.; Sweygers, N.; Al-Salem, S.; Appels, L.; Aminabhavi, T.M.; Dewil, R. Biochar for Soil Applications-Sustainability Aspects, Challenges and Future Prospects. *Chem. Eng. J.* **2022**, *428*, 131189. [CrossRef]
49. Brassard, P.; Godbout, S.; Lévesque, V.; Palacios, J.H.; Raghavan, V.; Ahmed, A.; Hogue, R.; Jeanne, T.; Verma, M. Biochar for Soil Amendment. In *Char and Carbon Materials Derived from Biomass*; Elsevier: Amsterdam, The Netherlands, 2019; pp. 109–146.
50. Hussain, A.J.; Al-Taey, D.K.A.; Kadhum, H.J. Biochar Application Increases the Amount of Nitrogen, Phosphorus and Potassium in the Soil: A Review. *IOP Conf. Ser. Earth Environ. Sci.* **2023**, *1213*, 012023. [CrossRef]
51. Zhang, W.; Wei, J.; Guo, L.; Fang, H.; Liu, X.; Liang, K.; Niu, W.; Liu, F.; Siddique, K.H.M. Effects of Two Biochar Types on Mitigating Drought and Salt Stress in Tomato Seedlings. *Agronomy* **2023**, *13*, 1039. [CrossRef]
52. Gullap, M.K.; Severoglu, S.; Karabacak, T.; Yazici, A.; Ekinci, M.; Turan, M.; Yildirim, E. Biochar Derived from Hazelnut Shells Mitigates the Impact of Drought Stress on Soybean Seedlings. *N. Z. J. Crop Hortic. Sci.* **2024**, *52*, 19–37. [CrossRef]
53. Palansooriya, K.N.; Yang, Y.; Tsang, Y.F.; Sarkar, B.; Hou, D.; Cao, X.; Meers, E.; Rinklebe, J.; Kim, K.-H.; Ok, Y.S. Occurrence of Contaminants in Drinking Water Sources and the Potential of Biochar for Water Quality Improvement: A Review. *Crit. Rev. Environ. Sci. Technol.* **2020**, *50*, 549–611. [CrossRef]
54. Wang, J.; Wang, S. Preparation, Modification and Environmental Application of Biochar: A Review. *J. Clean. Prod.* **2019**, *227*, 1002–1022. [CrossRef]
55. Qian, K.; Kumar, A.; Zhang, H.; Bellmer, D.; Huhnke, R. Recent Advances in Utilization of Biochar. *Renew. Sustain. Energy Rev.* **2015**, *42*, 1055–1064. [CrossRef]
56. Siipola, V.; Pflugmacher, S.; Romar, H.; Wendling, L.; Koukkari, P. Low-Cost Biochar Adsorbents for Water Purification Including Microplastics Removal. *Appl. Sci.* **2020**, *10*, 788. [CrossRef]
57. Adilina, I.B.; Widjaya, R.R.; Hidayati, L.N.; Supriadi, E.; Safaat, M.; Oemry, F.; Restiawaty, E.; Bindar, Y.; Parker, S.F. Understanding the Surface Characteristics of Biochar and Its Catalytic Activity for the Hydrodeoxygenation of Guaiacol. *Catalysts* **2021**, *11*, 1434. [CrossRef]
58. Longo, L.; Taghavi, S.; Riello, M.; Ghedini, E.; Menegazzo, F.; Di Michele, A.; Cruciani, G.; Signoretto, M. Waste Biomasses as Precursors of Catalytic Supports in Benzaldehyde Hydrogenation. *Catal. Today* **2023**, *420*, 114038. [CrossRef]
59. Longo, L.; Taghavi, S.; Ghedini, E.; Menegazzo, F.; Di Michele, A.; Cruciani, G.; Signoretto, M. Selective Hydrogenation of 5-Hydroxymethylfurfural to 1-Hydroxy-2,5-hexanedione by Biochar-Supported Ru Catalysts. *ChemSusChem* **2022**, *15*, e202200437. [CrossRef]
60. Wang, H.; Chang, G.; Qi, P.; Li, X.; Guo, Q. Preparation of Aromatic Hydrocarbons from Catalytic Pyrolysis of Microalgae/Palm Kernel Shell Using PKS Biochar-Based Catalysts. *Energy Fuels* **2019**, *33*, 379–388. [CrossRef]

61. Herrera, K.; Morales, L.F.; López, J.E.; Montoya-Ruiz, C.; Muñoz, S.; Zapata, D.; Saldarriaga, J.F. Biochar Production from Tannery Waste Pyrolysis as a Circular Economy Strategy for the Removal of Emerging Compounds in Polluted Waters. *Biomass Convers. Biorefin.* **2024**, *14*, 22867–22880. [CrossRef]
62. Lee, J.; Kim, K.H.; Kwon, E.E. Biochar as a Catalyst. *Renew. Sustain. Energy Rev.* **2017**, *77*, 70–79. [CrossRef]
63. Guo, F.; Dong, Y.; Dong, K.; Xu, L.; Liu, S.; Qiao, Q.; Wei, H.; Wang, Y. Role of Biochar-Based Catalysts in Microwave-Induced Biomass Pyrolysis: Structural Properties and Modification with Fe-Series Metals. *Fuel* **2023**, *341*, 127769. [CrossRef]
64. Tisserant, A.; Cherubini, F. Potentials, Limitations, Co-Benefits, and Trade-Offs of Biochar Applications to Soils for Climate Change Mitigation. *Land* **2019**, *8*, 179. [CrossRef]
65. Ghaffar, A.; Zhu, X.; Chen, B. Biochar Composite Membrane for High Performance Pollutant Management: Fabrication, Structural Characteristics and Synergistic Mechanisms. *Environ. Pollut.* **2018**, *233*, 1013–1023. [CrossRef]
66. Haykiri-Acma, H.; Yaman, S.; Kucukbayrak, S. Effects of Torrefaction on Lignin-Rich Biomass (Hazelnut Shell): Structural Variations. *J. Renew. Sustain. Energy* **2017**, *9*, 063102. [CrossRef]
67. Zinnanti, C.; Schimmenti, E.; Borsellino, V.; Paolini, G.; Severini, S. Economic Performance and Risk of Farming Systems Specialized in Perennial Crops: An Analysis of Italian Hazelnut Production. *Agric. Syst.* **2019**, *176*, 102645. [CrossRef]
68. Pagliero, M.; Bottino, A.; Comite, A.; Costa, C. Novel Hydrophobic PVDF Membranes Prepared by Nonsolvent Induced Phase Separation for Membrane Distillation. *J. Membr. Sci.* **2020**, *596*, 117575. [CrossRef]
69. Pagliero, M.; Comite, A.; Soda, O.; Costa, C. Effect of Support on PVDF Membranes for Distillation Process. *J. Membr. Sci.* **2021**, *635*, 119528. [CrossRef]
70. Sanz, J.M.; Jardines, D.; Bottino, A.; Capannelli, G.; Hernández, A.; Calvo, J.I. Liquid–Liquid Porometry for an Accurate Membrane Characterization. *Desalination* **2006**, *200*, 195–197. [CrossRef]
71. Calvo, J.I.; Bottino, A.; Capannelli, G.; Hernández, A. Comparison of Liquid–Liquid Displacement Porosimetry and Scanning Electron Microscopy Image Analysis to Characterise Ultrafiltration Track-Etched Membranes. *J. Membr. Sci.* **2004**, *239*, 189–197. [CrossRef]
72. Zhang, Y.; Tang, Y.; Yan, R.; Li, J.; Li, C.; Liang, S. Removal Performance and Mechanisms of Aqueous Cr (VI) by Biochar Derived from Waste Hazelnut Shell. *Environ. Sci. Pollut. Res.* **2023**, *30*, 97310–97318. [CrossRef]
73. Pang, C.H.; Lester, E.; Wu, T. Influence of Lignocellulose and Plant Cell Walls on Biomass Char Morphology and Combustion Reactivity. *Biomass Bioenergy* **2018**, *119*, 480–491. [CrossRef]
74. Kwiatkowski, M.; Broniek, E. An Analysis of the Porous Structure of Activated Carbons Obtained from Hazelnut Shells by Various Physical and Chemical Methods of Activation. *Colloids Surf. A Physicochem. Eng. Asp.* **2017**, *529*, 443–453. [CrossRef]
75. Zhou, X.-L.; Zhang, H.; Shao, L.-M.; Lü, F.; He, P.-J. Preparation and Application of Hierarchical Porous Carbon Materials from Waste and Biomass: A Review. *Waste Biomass Valorization* **2021**, *12*, 1699–1724. [CrossRef]
76. Sun, J.; Jayakumar, A.; Díaz-Maroto, C.G.; Moreno, I.; Fermoso, J.; Mašek, O. The Role of Feedstock and Activation Process on Supercapacitor Performance of Lignocellulosic Biochar. *Biomass Bioenergy* **2024**, *184*, 107180. [CrossRef]
77. Baldassin, D.; Longo, L.; Menegazzo, F.; Bittencourt, C.; Padervand, M.; Signoretto, M. Co-Pyrolysis of Leather Shaving Waste and Rice Husk for Hybrid Palladium-Supported Biochar Catalysts in Hydrogenation Reactions. *Mater. Today Sustain.* **2025**, *31*, 101127. [CrossRef]
78. Pagliero, M.; Comite, A.; Soda, O.; Costa, C. Influence of Carbon-Based Fillers on Photoactive Mixed Matrix Membranes Formation. *J. Membr. Sci.* **2022**, *658*, 120752. [CrossRef]
79. Qadir, D.; Mukhtar, H.; Keong, L.K. Mixed Matrix Membranes for Water Purification Applications. *Sep. Purif. Rev.* **2017**, *46*, 62–80. [CrossRef]
80. Pagliero, M.; Alloisio, M.; Costa, C.; Firpo, R.; Mideksa, E.A.; Comite, A. Carbon Black/Polyvinylidene Fluoride Nanocomposite Membranes for Direct Solar Distillation. *Energies* **2022**, *15*, 740. [CrossRef]
81. Eljaddi, T.; Cabassud, C. Wetting-Based Comparison of Ag, Carbon Black, and MoS2 Composite Membranes for Photothermal Membrane Distillation. *Membranes* **2023**, *13*, 780. [CrossRef] [PubMed]
82. Nassar, L.; Hegab, H.M.; Kharraz, J.A.; An, A.K.; Al Marzooqi, F.; El Fadel, M.; Hasan, S.W. Enhanced Solar Desalination with Photothermal Hydrophobic Carbon Nanotube-Infused PVDF Membranes in Air-Gap Membrane Distillation. *Desalination* **2024**, *592*, 118142. [CrossRef]
83. Zhang, Q.; Xu, H.; Lu, W.; Zhang, D.; Ren, X.; Yu, W.; Wu, J.; Zhou, L.; Han, X.; Yi, W.; et al. Properties Evaluation of Biochar/High-Density Polyethylene Composites: Emphasizing the Porous Structure of Biochar by Activation. *Sci. Total Environ.* **2020**, *737*, 139770. [CrossRef]
84. Cai, J.; Hu, N.; Wu, L.; Liu, Y.; Li, Y.; Ning, H.; Liu, X.; Lin, L. Preparing Carbon Black/Graphene/PVDF-HFP Hybrid Composite Films of High Piezoelectricity for Energy Harvesting Technology. *Compos. Part A Appl. Sci. Manuf.* **2019**, *121*, 223–231. [CrossRef]
85. Bottino, A.; Capannelli, G.; Munari, S.; Turturro, A. High Performance Ultrafiltration Membranes Cast from LiCl Doped Solutions. *Desalination* **1988**, *68*, 167–177. [CrossRef]

86. Woo, Y.C.; Kim, Y.; Shim, W.G.; Tijing, L.D.; Yao, M.; Nghiem, L.D.; Choi, J.S.; Kim, S.H.; Shon, H.K. Graphene/PVDF Flat-Sheet Membrane for the Treatment of RO Brine from Coal Seam Gas Produced Water by Air Gap Membrane Distillation. *J. Membr. Sci.* **2016**, *513*, 74–84. [CrossRef]
87. Wang, M.; Wang, Z.; Li, N.; Liao, J.; Zhao, S.; Wang, J.; Wang, S. Relationship between Polymer-Filler Interfaces in Separation Layers and Gas Transport Properties of Mixed Matrix Composite Membranes. *J. Membr. Sci.* **2015**, *495*, 252–268. [CrossRef]